

CSP plants with thermocline thermal energy storage and integrated steam generator - Techno-economic modeling and design optimization

Original

CSP plants with thermocline thermal energy storage and integrated steam generator - Techno-economic modeling and design optimization / Pizzolato, Alberto; Donato, F.; Verda, Vittorio; Santarelli, Massimo; Sciacovelli, Adriano. - In: ENERGY. - ISSN 0360-5442. - 139:(2017), pp. 231-246. [10.1016/j.energy.2017.07.160]

Availability:

This version is available at: 11583/2684847 since: 2017-11-14T17:01:54Z

Publisher:

Elsevier Ltd

Published

DOI:10.1016/j.energy.2017.07.160

Terms of use:

This article is made available under terms and conditions as specified in the corresponding bibliographic description in the repository

Publisher copyright

(Article begins on next page)

CSP plants with thermocline thermal energy storage and integrated steam generator – Techno-economic modeling and design optimization

A. Pizzolato^a, F. Donato^b, V. Verda^a, M. Santarelli^a, A. Sciacovelli^c

^aDepartment of Energy, Politecnico di Torino, Corso Duca degli Abruzzi 24, 10129, Torino, Italy, alberto.pizzolato@polito.it, 0110904478

^bENEA UTRINN Via Anguillarese 301, 00123 Rome, Italy

^cSchool of Chemical Engineering., Birmingham Centre for Energy Storage (BCES), University Of Birmingham, UK

Abstract

Although CSP has reached technological maturity, high capital investment and specific electricity cost remain the major development barriers. To reduce them, highly efficient, integrated, and cheaper CSP components are urgently needed. In this paper, we investigate a novel CSP plant configuration with a single-tank Thermal Energy Storage (TES) fully integrated with the steam generator.

The objective of this research is twofold: i) provide a reliable model of single-tank thermal storages with integrated steam generator; ii) identify two optimized CSP plant designs to achieve best energetic and economic performances. To achieve these aims we developed a numerical model of the main system components and validated it against experimental data. This model was then integrated in a full simulation and heuristic design optimization of the plant.

The results revealed that the system proposed can generate electricity in middle-Italy (Rome) at a cost of 230.25 \$/MWh with a 15% reduction compared to the double tank option. Furthermore, if cogeneration is used to recover the waste heat, this system is an interesting option for users such as small districts, university campuses and hospitals. In the latter case, the optimized system pays off in 6 years and covers 80% of the heating and cooling requirements.

Highlights

- A novel CSP plant with thermocline TES and integrated steam generator is modeled in details
- The solar field and the integrated TES models are validated with experimental data
- The single tank configuration lowers the LEC of 42 \$/MWh

- Cogeneration lowers the LEC of 28%

Keywords: Concentrated Solar Power; Integrated Steam Generator; Molten Salts; Techno-economic Optimization; Thermocline Energy Storage;

Nomenclature

Latin letters

A	Area [m^2]
C	Cost [\$]
c_p	Specific Heat [$\frac{J}{kgK}$]
C_y	Yearly cost [$\frac{\$}{year}$]
d	Diameter [m]
E	Yearly Electrical energy [$\frac{MWh}{year}$]
\dot{E}	Electrical power [W]
e	Specific kinetic energy [$\frac{J}{kg}$]
Eu	Euler number [-]
FIT	Feed-In Tariff [$\frac{\$}{MWh}$]
f_{labor}	Labor cost index ratio [-]
$f_{M\&S}$	Marshall & Swift cost index ratio [-]
h	Specific enthalpy [$\frac{J}{kg}$]
k	Thermal conductivity [$\frac{W}{m K}$]
k_l	Geometric factor for helicoidal heat exchangers [-]
L	Length [m]
LEC	Levelized Electricity Cost [$\frac{\$}{MWh}$]
m	Mass flow rate [$\frac{kg}{s}$]
n	Scale factor [-]
Nu	Nusselt number [-]
p	Pressure [Pa]
Pr	Prandtl number [-]

Q	Yearly Thermal Energy $\left[\frac{\text{GJ}}{\text{year}}\right]$
\dot{Q}	Thermal power [W]
R	Revenues [\$]
Re	Reynolds number [-]
R_y	Yearly revenues $\left[\frac{\$}{\text{year}}\right]$
S	Characteristic size [-]
$SPBT$	Simple Payback time [years]
T	Temperature [K]
t	Time [s]
$TCLF$	Thermal Load Capacity Factor [-]
U	Global heat transfer coefficient $\left[\frac{\text{W}}{\text{m}^2\text{K}}\right]$
th	Thickness [m]

Greek letters

α	Heat transfer coefficient $\left[\frac{\text{W}}{\text{m}^2\text{K}}\right]$
η	Efficiency [-]
ρ	Density $\left[\frac{\text{kg}}{\text{m}^3}\right]$

Subscripts

abs	Absorbed
b	Buoyancy
bc	Boundary condition
bl	Boling
cont	Contingencies
dec	Decommissioning
dir	Direct
ec	Economizer
el	Electrical
ev	Evaporator
f	Friction
Fo	Fouling
FW	Feed-water
h	Hydraulic

HTF	Heat Transfer Fluid
i	Internal
in	Incoming
inv	Investment
lam	Laminar
ls	Liquid-Solid phase transition
MS	Molten Salts
nom	Nominal
o	External
O&M	Operation and Maintenance
out	Outgoing
ref	Reference
SF	Solar Field
sh	Superheater
sol	Solar
t	Tube
th	Thermal
turb	Turbulent
y	Yearly

1 Introduction

Despite having been under investigation for several decades, Concentrated Solar Power (CSP) is still hardly competitive with conventional fossil-based power plants and the expected market development in the Mediterranean region remains an unfulfilled promise. The high upfront investment cost and the difficult siting [1] are the two major barriers to a rising share of CSP in the future energy mix. It is thus clear that the primary focus of future research should be the reduction of both the investment cost and the specific cost of electricity, which will extend the CSP market also to mid-size plants located at intermediate latitudes.

The first step in this direction is the simplification of the power plant loop. In this regard, ENEA (Italian National Agency for New Technologies, Energy and Sustainable Economic Development) has promoted [2] the use of a thermocline (i.e. single-tank) Thermal Energy Storage (TES) with an integrated Steam Generator (SG) submerged in the heat storage medium. The plant can be further simplified through the use of the molten salts mixture, which was commonly found as heat storage

medium, also as the Heat Transfer Fluid [3] with consistent benefits to the efficiency of the power cycle.

The submerged steam generator technology is well-known within the nuclear community and many models have been developed in the past. For instance Ref. [4] proposed a lumped parameter approach considering three regions (i.e. the subcooled, the boiling and the superheater region) with movable boundaries, while in Ref [5] the Authors refined the discretization to get a 1D finite volume approach[6]. However, only a few studies [7], considered the natural circulation on the coolant side, with a design close to the submerged steam generator proposed by ENEA. Furthermore, literature is rich in thermocline TES model. For instance, Yang and Garimella [8] investigated the performance of a molten salts thermocline tank filled with quartzite rock through a 2D axial-symmetric finite volume model; they show that the discharge efficiency raises for tanks with a high aspect ratio and operated at small Reynolds number. Strasser et al. [9] adopted a similar approach to show that the cycle efficiency can be further enhanced with a structured concrete network instead of conventional packed bed material. The use of latent heat storage in CSP has also been studied in great details: Nithyanandam et al. [10] studied the performance of a packed bed TES with encapsulated PCM during partial charging and discharging cycles while Fornarelli et al. [11] developed a detailed numerical model of a shell-and-tube TES with Phase Change Material showing that natural convection can be conveniently exploited to reduce the melting time. Despite this great availability of literature on the topic, only Ref. [12] studied the integrated storage-steam generator system. The great level of detail of their finite volume model makes it ideal for technology development but impractical for system analysis and plant optimization, which demand for more compact modeling approaches.

For what it concerns the reduction of the specific cost of electricity, a possible field of competitiveness improvement for small CSP is represented by polygeneration. The option of CSP-driven desalination has been widely investigated [13 14], since regions with high water scarcity generally have a large solar resource. Another interesting cogeneration option is the CSP-driven biomass gasification, which has lately received considerable attention in the scientific community [15]. On the other hand, it should be noted that only a few researchers [16, 17] have investigated the cogeneration of power, heating and cooling in a single CSP plant, which could be an ideal opportunity to enlarge the market of CSP to users like small districts, university campuses and hospitals.

We believe that the innovative match of these two concepts, i.e. the ENEA compact system and the cogeneration option, has the potential to open the doors of CSP to small-scale facilities in regions with moderate solar resources. In order to quantify this potential, in this paper we utilize the tools of

energy and economic analysis, which have been proficiently applied in the past to solar tower combined cycle [18, 19], parabolic through plants for process heat generation [20] and to CSP desalination plants [21].

This paper stems from the need of filling the literature gaps we highlighted in this introduction. Firstly, we aim at providing a reliable (i.e. validated with experimental data) and computationally cheap (i.e. suited for system-level annual simulations) modeling framework of the storage tank with integrated steam generator. Secondly, this paper has the objective of proposing two optimized designs of the small CSP cogeneration system as well as to analyze their performances. The first design is thought for an ideal thermal user and has the aim of establishing the potential of the technology. The second one is targeted to a specific user, i.e. a hospital, and has the aim to analyze the performances of the system when coupled with a real user in a real energy market.

2 The CSP cogeneration plant with thermocline TES and integrated Steam Generator

2.1 Power plant description

Figure 1 presents the system proposed by ENEA. The molten salts pump (MSP) circulates the “solar salt” (i.e. an eutectic mixture with 60 wt % NaNO_3 and 40 wt % KNO_3) from the storage tank into the receiver tubes of the Parabolic Trough Solar Collectors (PTSC) (streams 1, 2 and 3). Once the fluid reaches the desired temperature (stream 4), it is circulated back to the storage tank (stream 6). If the system conditions do not allow to reach the desired temperature the salts can be circulated back to the solar collectors with a by-pass valve (stream 5). The storage tank contains a steam generator, which is immersed in the molten salts; this sub-system is called Storage Tank with Integrated Steam Generator (STISG). The steam produced (stream 7) flows to the steam turbine and it is eventually condensed in the condenser (WCD) (stream 8). In cogeneration mode, the thermal power collected by the steam condenser (stream 11) is used to satisfy the thermal requirements of a heat consumer or can be fed to an Absorption Chiller Unit (ACU) to satisfy a cooling load. Finally, the Rankine cycle is closed with the use of a water pump (WP1).

In the following sections, a summary of the modelling approach of the three main subsystems of the plant is given, namely the solar field, the STISG and the power block.

2.2 Main assumptions

The following assumptions have been made to model the plant:

- The maximum design temperature in the receiver is set to 550 °C. This value is suggested based on the experience matured at the 5 MW Archimede plant in Priolo Gargallo [22]. At higher temperatures, alkaline hydroxides and carbonates are produced at higher rate. These

species present a limited solubility in molten nitrates and precipitate rapidly yielding to pipes and valves occlusion.

- The high pressure level of the steam cycle has been fixed to 40 bar.
- The condenser minimum driving temperature difference, i.e. at the pinch point, has been set to 10 °C.
- The temperature required by the waste heat recovery unit (stream 12) has been set equal to 90 °C.
- The efficiency of the heat distribution system is set to 90% and the Coefficient of Performance of the absorption chiller to 60%, as suggested as a reasonable value for single effect Water-LiBr absorption machines (e.g. in [23]). This means that, in winter, 90% of the recovered heat is available as heating power, while, in summer, 60 % of the recovered is available as cooling power. Distribution losses are neglected.

3 Mathematical modelling of the power plant components

3.1 Solar field

3.1.1 Components description and Model

We have modeled a concentrator similar to the one already in operation at the Archimede plant [22]. The parabolic through reflector is a 12.5 m long parabolic mirror with 5.76 m of aperture and a focal height of 2.01 m. It sustains a 4.06 m long receiver tube consisting of an absorber inside a glass envelope with bellows at either end. The absorber is a stainless steel tube (70 mm in diameter) which is treated with selective coating to obtain a high absorptance in the solar energy spectrum, and low emittance in the infrared (i.e. 95% and 7.3% respectively from manufacturer specifications). The glass envelope (125 mm in diameter) is made of Pyrex and guarantees a transmittance higher than 96% in the full range of operating temperatures. The annulus space between the absorber and the glass envelope is under vacuum (1×10^{-4} mbar) to reduce thermal losses.

In the present work, the analytical equations of Ref.[24] are used for the solar position and the optical model of the receiver while a more detailed approach is followed for the thermal model of the receiver tube. A quasi 1D model is implemented: the receiver is discretized along the axial direction and, for each of the finite volume, a thermal balance is written considering non-advective heat transfer (i.e. conduction and radiation) only in the radial direction. This approach is widely used for the simulation of thermal systems of this type [24, 25]

Specifically, the formulation presented in Ref. [25] is considered: assuming steady-state and for a negligible change in potential energy we can write:

$$\dot{Q}_{net} = \dot{m}_{HTF} (h_{in} + e_{in} - h_{out} - e_{out}) \quad (1)$$

\dot{Q}_{net} is the radiative power effectively transferred to the heat transfer fluid and can be calculated as:

$$\dot{Q}_{net} = \dot{Q}_{abs} - \dot{Q}_{losses} \quad (2)$$

In steady-state conditions, the concentrated radiation absorbed on the surface of the absorber tube can be either transmitted to the heat transfer fluid or rejected towards the environment. In the first case, we have a series of the following thermal resistances (Fig. 2)

- Conduction from the outer surface of the absorber tube to the inner surface of the absorber tube
- Convection from the inner surface of the absorber tube the heat transfer fluid

In the second case, the thermal power path is the following (Fig. 2):

- Radiation/convection heat transfer from the outer surface of the absorber tube to the inner surface of the glass envelope
- Conduction heat transfer across the glass envelope
- Radiation/convection heat transfer from the external surface of the glass envelope towards the environment

The thermal properties of the materials and the correlations proposed in [25] were used for the calculation of the heat transfer coefficients. The irradiance data were obtained from the HelioClim3 database [26] and the wind speed and ambient temperature data from the EnergyPlus database [27], both providing data with a 15 minutes sampling.

3.1.2 Experimental validation

The test bench consists of a 50 meters parabolic trough solar field, similar to the one described in the modeling section of this paper. The experimental string is composed by 4 reflectors in series. Four thermocouples are soldered on the external surface of the receiver tube at each joint between consecutive reflectors. Two submerged thermocouples are placed at the inlet and at the outlet of the experimental facility, i.e. at $x = 0$ m and at $x = 50$ m respectively. The soldered thermocouples provide a highly varying measurement along the angular coordinate which cannot be accounted for in our quasi 1D model. Hence, only the measurements provided by the submerged thermocouples is used. The measurement at $x = 0$ m provides the inlet boundary condition while the measurement at $x = 50$ m is used to validate the model. Figure 3 compares temperature measured at $x = 50$ m with values predicted by our numerical model. The average mass flow rate during the test is 6.39 kg/s with a standard deviation of 0.23 kg/s. The largest difference between experimental and numerical results arises when the inlet temperature is varied over the duration of the test because the model does not account for transient effect, while

a good approximation is visible during steady-state conditions. Nevertheless, a steady-state model remains suitable to reproduce the normal operating conditions of a commercial CSP plant, where the mass flow rate is varied by the control system to maintain a constant temperature levels across the receiver tubes. The average first law efficiency is calculated as 0.54 with a standard deviation of 0.05.

3.2 Storage tank with integrated steam generator

3.2.1 Component description and model

The steam generator is a once-through counterflow shell-and-tube heat exchanger with a helicoidal tube bundle: on the shell-side, in an annulus-shaped channel, the molten salts flow downward and, on the tube side, water flows upward becoming superheated steam. This heat exchanger operates in natural circulation mode on the molten salts side thanks to the strong fluid; in fact, within the range of temperatures considered, the density of the fluid experiences nearly a 10% variation which is exploited as motion driving force.

Figure 4 schematically illustrates the STISG system for the small CSP cogeneration plant described in Section 2.

The temperature of fluids along the axial dimension of the steam generator are calculated with a one-dimensional finite volume numerical model [28] using a double iteration loop to solve the natural circulation problem (Figure 5):

1. The molten salts mass flow is guessed
2. The outlet temperature of the molten salts (bottom side of the steam generator) is guessed
3. The thermal problem is solved following a first-order upwind approximation on the water side until the temperatures of the two fluids in the upper side of the steam generator are obtained, i.e. the molten salts inlet temperature and the steam outlet temperature
4. The calculated inlet temperature of the molten salts is compared with the boundary condition. If the convergence criterion is not met, a new outlet temperature is calculated and the code returns to step 3. Otherwise, the algorithm is allowed to proceed to step 5.
5. The pressure drop on the molten salts side is calculated and it is compared to the buoyancy pressure difference. If the convergence criterion is not met, the algorithm calculates a new mass flow and returns to step 1. Otherwise the algorithm returns the solution.

Convergence criteria are written as absolute differences where the tolerances, i.e. ε_{th} and ε_{fd} , are set to 10^{-3} °C and 10^{-2} Pa for the thermal and fluid-dynamic model respectively. The heat transfer and pressure drop correlations presented in [28] were used for the calculations and are briefly summarized below.

The water internal heat transfer coefficient in the economizer and in the superheater are calculated with the Dittus-Boelter [29] and the Heinmen correlation [30] respectively. In formulas:

$$Nu_{ec,w} = 0.023 Re^{0.8} Pr^{0.4} \quad (3)$$

$$Nu_{sh,w} = 0.133 Re^{0.84} Pr^{0.333} \quad (4)$$

In the evaporating section, the Chen correlation [31] was used to calculate the heat transfer coefficient:

$$\alpha_{ev,w} = \alpha_{bl} S + \alpha_{ls} F \quad (5)$$

where the suppression factor S accounts for the reduction of the boiling heat transfer coefficient when convective boiling becomes dominant; F is the Chen phase multiplier. For further details the reader is referred to the original work of Chen [31].

On the molten salts side, the steam generator can be modeled as a bank of helicoidal tubes in cross-flow. The Nusselt number was calculated combining a turbulent and a laminar term in the following way [30]:

$$Nu_{MS} = 0.3 + \sqrt{Nu_{lam}^2 + Nu_{turb}^2} \quad (6)$$

where:

$$\circ \quad Nu_{lam} = 0.664 \sqrt{Re} Pr^{1/3} \quad (7)$$

$$\circ \quad Nu_{turb} = \frac{0.037 Re^{0.8} Pr}{1 + 2.433 Re^{-0.1} (Pr^{2/3} - 1)} \quad (8)$$

Once the internal and external heat transfer coefficients, i.e. α_i and α_o , are known the global heat transfer coefficient of the j -th volume U_j is obtained as:

$$U_j = \left(\frac{1}{\alpha_i} + \frac{r_i}{r_o \alpha_o} + \frac{r_i \log \left(\frac{r_o}{r_i} \right)}{k_t} \right)^{-1} \quad (9)$$

The heat transfer rate exchanged in the j -th volume \dot{Q}_j is hence calculated as follows:

$$\dot{Q}_j = U_j S_j (T_{FW_j} - T_{MS_j}) \quad (10)$$

The temperature profiles on the water and molten salts side are then calculated according to an upwind scheme. For the economizer and superheater sections we write:

$$T_{FW_{j+1}} = T_{FW_j} - \frac{\dot{Q}_j}{m_{FW} c_{p,FW}} \quad (11)$$

In the evaporating section, the water temperature is always equal to the saturation temperature and we monitor the evolution of the vapor fraction x_{FW} as following:

$$x_{FW_{j+1}} = x_{FW_j} + \frac{\dot{Q}_j}{m_{FW} h_{fg}} \quad (12)$$

On the molten salts side we have:

$$T_{MS_{j+1}} = T_{MS_j} - \frac{\dot{Q}_j}{m_{MS} c_{p,MS}} \quad (13)$$

The correlations for a bank of helicoidal tubes in cross flow proposed in [30] are used for fluid-dynamic calculations. After the preliminary calculation of the geometrical factor k_1 , the Euler number Eu is obtained as follows:

$$\frac{Eu}{k_1} = 0.263 + \frac{0.867 \cdot 10^{-2}}{Re} - \frac{2.02}{Re^2} \quad \text{for } Re < 2 \cdot 10^3 \quad (14)$$

$$\frac{Eu}{k_1} = 0.235 + \frac{0.198 \cdot 10^{-4}}{Re} - \frac{0.124 \cdot 10^8}{Re^2} + \frac{0.312 \cdot 10^{11}}{Re^3} - \frac{0.274 \cdot 10^{14}}{Re^4} \quad \text{for } 2 \cdot 10^3 \leq Re < 2 \cdot 10^6 \quad (15)$$

As far as the modeling of the stratification in the TES is concerned, we consider the Reynolds-averaged version of the turbulent Navier-Stokes equations. Mathematically:

$$\frac{\partial \rho}{\partial t} + \frac{\partial \rho u_j}{\partial x_j} = 0 \quad (16)$$

$$\frac{\partial \rho u_i}{\partial t} + \frac{\partial}{\partial x_j} (\rho u_j u_i) = -\frac{\partial P}{\partial x_i} + \frac{\partial \sigma_{ij}}{\partial x_j} + F_i \quad (17)$$

$$\frac{\partial \rho E}{\partial t} + \frac{\partial}{\partial x_j} (\rho u_j H) = \frac{\partial}{\partial x_j} (u_i \sigma_{ij}) - \frac{\partial}{\partial x_j} \left(\left(\frac{\mu}{Pr} + \frac{\mu_T}{Pr_t} \right) \left(\frac{\partial T}{\partial x_j} \right) \right) \quad (18)$$

where σ_{ij} is the tensor of viscous stresses, S_{ij} is the tensor of shear stresses and H is the total enthalpy. The governing equations are converted to algebraic equations using the finite-elements method with 2nd order Lagrange finite elements for the velocity field and linear elements for the pressure and temperature fields. Closure of the turbulent equations is provided through $ak - \omega$ model.

The CFD approach is too demanding for system-level simulations. Hence, in this paper we use a logistic distribution function to represent the non-dimensional molten salts temperature profile of a vertical fluid column inside the tank. The function was parametrized statistically, using 18 Computational Fluid-Dynamic (CFD) simulations. This approach proved to be extremely convenient for the adaptation of CFD results to annual system-level simulation and optimization. For an extensive discussion on the reduction methodology, the reader is referred to [32]

3.2.2 Experimental validation

Figure 6(a) shows the results for the steam generator operated with 85% of the nominal mass flow rate (0.11 kg/s) of water and for a molten salts inlet temperature of 520 °C. The molten salts side results show very good agreement with experimental data. The skin temperature (i.e. metal temperature of the external surface of the receiver tube) calculation is quite accurate in the evaporating section while it shows a non-negligible deviation in the superheating section.

However, the trend is well reproduced and the large error is mainly due to the sharp increase of the water temperature in the superheating section. A small difference of the water mass flow, in fact, can result in large relative errors.

Figure 6.(b) and Figure 6.(c) show the results obtained with a water mass flow 10% and 20% higher than the nominal value. Differently from the previous case, the water side is quite well approximated except for the top section of the steam generator.

In all the tests conducted we obtained an average absolute error in the molten salts temperature of 3.16 °C with a standard deviation of 3.22 °C. Furthermore, an excellent agreement between predicted and experimental inlet/outlet temperatures of water and molten salts is achieved, thus the model can be confidently used for system-level simulations.

The validation of the CFD model is an essential step of the methodology proposed in the present paper, allowing to proceed with multiple simulations in different conditions and to characterize the reduced model (i.e. the logistic function) by statistical means. Validation has been performed using experimental data taken from 14 thermocouples equally spaced every 10 cm on a long rod that is immersed vertically in the tank at $r = 0.5$ m.

The validation of the discharging process is shown in Figure 7(a). Solid lines are the results obtained by the CFD simulation, while starred indicators are the experimental data. The average absolute error is 1.18 °C with a standard deviation of 2.53 °C. As far as the standby process is concerned, the results are compared for a total period of approximately 27.8 hours. Referring to Figure 7(b), starred red markers indicate the experimental results, while blue solid lines are obtained by the CFD simulation. Very good agreement is reached in the upper part of the tank where the rate of temperature drop in time is perfectly predicted by the CFD model. Also in this case, the comparison with experimental data is satisfactory with an average absolute error of 1.91 °C and a standard deviation of 3.14 °C.

The reduced model was then tested against the CFD simulations to verify its accuracy. The prediction achieved through the two modeling approaches are compared in Figure 8 for both a charging and a discharging process. The results obtained with the reduced model show a nearly perfect agreement with the CFD ones. The interested reader is advised to examine [32], for the full details and the potential applications of this model reduction approach.

3.3 Power block

The power block sub-system includes three main components: the steam turbine, the steam condenser and the feedwater pump.

The thermodynamic performance of the steam turbine is modelled according to Medina Flores et al. [33]. The Authors proposed to write the isentropic efficiency of the turbine as a function of the steam pressure at the inlet and at the outlet section of the turbine.

In summary, the electrical power output can be written as:

$$\dot{E}_{el} = \frac{1}{\beta} (\dot{m}(h_1 - h_{2,iso}) - \alpha) \quad (19)$$

where α and β are two pressure-dependent fitting parameters calculated as proposed in the original reference.

According to Ref. [33], the power output of the turbine during the startup can be obtained through the use of a startup factor $F_{startup}$ in the following way:

$$\dot{E}_{el} = F_{startup}(t) \dot{E}_{nom} \quad (20)$$

The correction factor ranges from 0 to 1, at the beginning and at the end of the startup process respectively, and increases quadratically in time. It can be calculated with:

$$F_{startup}(t) = \left(\frac{t_{sin ceStartup}(t)}{t_{startup}} \right)^2 \quad (21)$$

In the framework of this paper, $t_{startup}$ is set to one hour.

The condenser considered in the present work is a shell-and-tube heat exchanger as the one described in Ref.[34]. Its axial coordinate is discretized and in each of the volume considered, the thermal power \dot{Q} is calculated by means of an energy balance.

The global heat transfer coefficient is determined as follows [34]:

$$U = \left(R_{fo} + \left(\frac{1}{\alpha_i} + R_{fi} \right) \frac{d_o}{d_i} + \frac{th_t}{k_t} \frac{d_o}{D_m} + \frac{1}{h_o} \right)^{-1} \quad (22)$$

Here, R_{fi} is the fouling factor, d is the diameter, th_t is the tube thickness, k_t is the tube conductivity and α is the heat transfer coefficient. Subscripts i and o apply for internal and external side of the tube respectively. D_m is mean diameter calculated as follows:

$$D_m = \frac{d_o - d_i}{\ln \left(\frac{d_o}{d_i} \right)} \quad (23)$$

Moving to the feedwater pump, the approach followed is the one of Pelster[35], where the power consumption of the device \dot{E}_{pump} is calculated with:

$$\dot{E}_{pump} = \frac{1}{\eta_h} \dot{m}_{FW} \left(\frac{\Delta p}{\rho} \right) \quad (24)$$

Following the approach proposed by the same author, the pump outlet temperature T_{out} is computed as [34]:

$$T_{out} = T_{in} + \frac{(1 - \eta_h) \dot{E}_{pump}}{\dot{m} \bar{c}_p} \quad (25)$$

Due to the high degree of maturity of these conventional components, the power block model is considered reliable enough, and in this case, no experimental validation is performed.

4 Cases considered

In this paper, two different optimization cases are considered:

- CASE 1: THE MODULAR DESIGN: which has the aim of showing the potential of the technology and the advantages of cogeneration in a deliberately general setup
- CASE 2: THE TAILORED DESIGN, which has the aim of demonstrating the competitiveness of the technology in a specific market with real thermal users.

The modular design is a single-objective optimization of the system configuration in order to minimize the Levelized Cost of Electricity. In this case, we fix the size of the plant to 1 MW_e, which should fit many mid-size industrial users and we consider the system to be located in Rome. As far as cogeneration is concerned, since the objective of this case is to quantify the maximum economic advantages that cogeneration can bring, we consider an ideal thermal load where waste heat is always fully utilized to satisfy heating and cooling needs.

On the other hand, the tailored design is a double objective optimization built to minimize the payback time and to maximize the fraction of user's heating and cooling load satisfied by the solar system, i.e. the Thermal Load Capacity Factor (TLCF). Hence, in this case, we consider both a real thermal load and a real power market. The user in question is a 500 beds hospital, located in middle-Italy. The name of the hospital cannot be revealed due to non-disclosure agreements. The heating load is completely satisfied by a simple natural gas boiler while cooling is obtained through a hybrid system where vapor compression chillers are used for base load and gas absorption chillers are used for peak shaving and security of supply. The absorption machines are single-effect water-LiBr chillers. Their operation is modeled with a constant COP of 60 %, as suggested in [23] for this type of machines. Since the cooling system is already in place and its installation is rather recent (dated 2013), we do not account for it in our economic analysis.

The fraction of the building thermal load satisfied through natural gas is monitored through hourly readings of the meter. Figure 9(a) and 9(b) show the thermal load on a typical winter day and on a typical summer day respectively. These graphs are obtained by averaging the measurements over the season considered. In winter, two load peaks are visible, one in the morning around 7 am and one at night around 8 pm. The load is much steadier in summer where only small fluctuations are

visible between 1 pm and 8 pm. The cumulative power distribution in the year considered is given in Figure 9(c). A base load is well identified to be slightly more than 500 kW and the peak demand is roughly 2500 kW.

Compared to Case 1, the tailored design should include two additional design variables:

- The size of the power plant, which should fit the specific needs of the user
- The size of a hot water storage tank, which is needed to handle successfully possible mismatches between power block operations and the heating/cooling load

The building is located in a slightly populated area, with large ground availability for the installation of the solar field. The vicinity of the solar field makes the distribution thermal losses negligible.

5 Optimization setup

Evolutionary algorithms are acknowledged to be the most suitable choice for the optimization of complex energy systems, which often result in Mixed Integer highly Non-Linear Problems (MINLPs) with several non-feasible holes in the design space [36].

In this paper, we use the parallel implementation of the GA of the MATLAB Optimization Toolbox with a total of 10 decision variables (summarized in Table 1) and a population size of 50 individuals. The initial population is randomly generated in the feasible region.

Convergence is considered reached when the average L_2 norm step in the normalized objective(s) space drops below $1e-2$. This happened after a total of 52 and 62 generations for the 1st and 2nd case respectively.

The design variables are selected to enhance freedom in the design of the most relevant power plant components, i.e. the TES, the power block, the solar field, the steam generator and the waste heat utilization system.

Starting from the TES, the number of storage hours NH is an intuitive representation of the storage tank size. This value is the number of hours of continuous nominal operation that could be guaranteed to the power block during an ideal discharge process, i.e. starting from the tank fully charged at the maximum temperature and assuming no mixing or diffusion during the discharge. The aspect ratio of the tank is defined as the ratio of the tank diameter D to the tank height H and its choice is the trade-off between two competing phenomena: a large tank aspect ratio brings a small average Reynolds number of the molten salts during the charging and discharging phase which reduces thermocline degradation due to turbulence effects. On the other hand, a small tank aspect ratio, although reducing the area of contact with the cold and the hot fluid, brings more turbulent degradation.

We chose the design turbine power P_e as the representative variable for the power block. Once P_e is set, the remaining power block components are sized according to the design thermodynamic cycle obtainable through the assumptions outlined in Section 2.2.

Moving to the solar field, the solar multiple (SM) is defined as the ratio of the total mirror area to the "exact mirror area". This last quantity is the solar field aperture area required to deliver to the power cycle the thermal power needed to operate the turbine in nominal conditions. Besides the total area, the optimal number of collectors per string n_{coll} should also be carefully identified: this design variable affects the average heat transfer fluid velocity, whose value is a tradeoff between heat transfer efficiency and pressure losses. Moreover, the orientation of the solar field is expected to play a major role on the annual performance of the system. The optimizer can vary this variable between 1 and 2, being the former the N-S orientation and the latter the E-W orientation. Finally, the solar field design has one more degree of freedom, the solar field spacing $d_{spacing}$ between adjacent strings of solar collectors. A too compact solar field design can yield a high self-shadowing effect between solar collectors and a consequent drop in the optical efficiency. On the other hand, a too far placement implicates a higher land cost.

Two design variables were identified for the steam generator: the number of tubes n_{tubes} and the height H . The bounds have been set according to some preliminary design performed by ENEA in the framework of the OPTS European project [37].

In Case 2 we decided to evaluate the installation of a hot water storage tank placed right after the condenser. Hence, a new design variable was created that is the water storage capacity quantified in terms of full load hours NH_{water} of the heating/cooling system. This quantity is defined as the number of hours of continuous operation guaranteed to the heating and cooling systems at maximum load.

As far as the objective functions are concerned, we consider:

- The Levelized Electricity Cost (LEC) for Case 1
- The Simple Pay-Back Time (SPBT) for Case 2
- The Thermal Load Capacity Factor (TLCF) for Case 2

The LEC was preferred over other economic indicators, e.g. the Net Present Value (NPV), for its great adoption in the field of CSP, hence making comparison with other studies straightforward. Also please note that the plant operator and the thermal user are considered two different entities in this study, hence any purchase for the electrical grid or consumption of back-up natural gas by the latter is disregarded.

The first two objectives, i.e. the ones accounting for the economic performance of the plant, are defined as:

$$LEC = \frac{CRF \cdot C_{inv} + C_{y,O\&M} + C_{y,dec} + C_{y,cont} - R_{y,heat\&cold}}{E_y} \quad (26)$$

$$SPBT = \frac{C_{inv}}{R_{y,electricity} + R_{y,heat\&cold} - C_{y,O\&M} - C_{y,dec} - C_{y,cont}} \quad (27)$$

where:

- CRF [-] is the annualization factor that can be computed as:

$$CRF = \frac{i(1+i)^n}{(1+i)^n - 1} + k_{ins} \quad (28)$$

In the previous equation the interest rate i and insurance rate k_{ins} are set to 7% and 2% respectively as suggested in Ref. [35].

- $C_{inv}[\$]$ is the investment cost of the plant obtained summing the investment costs of all the components, i.e. $C_{inv} = \sum C_i$. The investment cost of the i^{th} component C_i is calculated through the use of cost functions, which stem from a best-fit on a wide range of market data and relate the cost of component to a specific size parameter S_i . Mathematically [35]:

$$C_i = c_{ref} \left(\frac{S_i}{S_{ref}} \right)^n f_{M\&S} \quad (29)$$

The adopted $f_{M\&S}$ index for the present study is the one of 2011 obtained from Ref. [38] and set to 1546.5. The full reference data of c_{ref} , S_{ref} , and n for the power block is obtained by [35], while the ones related to the solar field and the molten salts TES are gathered from [39]. The characteristic dimensions, their reference value and the specific reference costs of the components considered are listed in Table 2. The characteristic dimensions are obtained directly from the definition of the design variables. For more details on the cost function approach used to calculate the components investment costs, the reader is referred to [36, 44].

- $C_{y,O\&M} \left[\frac{\$}{year} \right]$ represents the Operation & Maintenance costs. We consider service contracts for groundkeeping, mirrors washing and water treatment, material maintenance for the equipment and operation cost due to personnel. All the data obtained through [39] are normalized on the plant electrical capacity to obtain a specific O&M cost.
- $C_{y,cont} \left[\frac{\$}{year} \right]$ and $C_{y,dec} \left[\frac{\$}{year} \right]$ refer to contingencies costs and decommissioning costs. In the present paper we follow the approach presented in Ref. [35] and set them to 10 % and 5 % respectively of the total project cost.

- $R_{y,heat\&cold} \left[\frac{\$}{year} \right]$ accounts for the revenues from the heat market considered as savings brought by the CSP cogeneration installation with respect to a conventional natural gas boiler and a H₂O-LiBr absorption chiller. In mathematical terms:

$$R_{y,heat\&cold} = p_{NG} \left(\frac{Q_{heat} + \frac{Q_{cold}}{COP_{ACU}}}{\eta_{boiler}} \right) = p_{NG} \frac{Q_{wasteHeat}}{\eta_{boiler}}$$

(30)

where the second equality sign holds only in case of complete sale of the plant waste heat on the market, i.e. case 1. We set the thermal efficiency of the typical natural gas boiler η_{boiler} to 90%, and the price of natural gas p_{NG} equal to 10.087 €/GJ, that is the market price for industrial users as set by the Italian Ministry of Development and Economic Resources [40].

- $R_{y,electricity} \left[\frac{\$}{year} \right]$ accounts for the revenues from the electricity market and it is calculated as:

$$R_{y,electricity} = p_e E \quad (31)$$

Where p_e is the price at which electricity is sold in the italian power market, which is determined by summing the fixed incentive of the Feed-In-Tariff (FIT) scheme and the liberalized price with which electricity producers are remunerated on the day-ahead market. Those last data are obtained on the GME (Italian Electricity Market manager) website [41] for the year 2014 while the incentive tariff is set according to the Italian Ministerial Decree of 6 Jul. 2012 to 320 €/MWh[42] .

Table 2 summarizes the most relevant data implemented in the economic model. For a more exhaustive breakdown at the component level, the reader is advised to consult [39].

The last objective function (i.e. TLCF) quantifies the performances of the CSP plant when used in cogeneration mode. It is calculated as:

$$TLCF = 1 - \frac{E_{backup}}{Q_{heat} + Q_{cold}} \quad (32)$$

that is the solar fraction of the annual heating and cooling demand.

6 Results and discussion

6.1 Case 1

Table 3 presents the optimized design specifications for Case 1. The optimal design presents a high value of solar multiple and storage tank size in order to increase the capacity factor of the steam

turbine. However, the optimal storage tank size and solar multiple are far from the upper bound set for the optimization routine. This means that an optimum is present in the range considered and that the marginal cost of adding storage capacity and more mirrors to the solar field does not pay off.

On the other hand, the number of collectors per string is maximum which means that increasing the length of the single string results in a higher annual yield of the solar field.

The height of the steam generator and the number of tubes selected are in close agreement with the preliminary design proposed by the manufacturer for the European Project OPTS. Finally, the optimal tracking axis orientation found is N-S which brings an 11% increase in the annual electricity yield of the unit square meter compared with E-W orientation.

The main annual energy flows and first-law efficiencies are summarized in Table 4. The proposed system in the optimized configuration generates 3864 MWh of electricity per year, which results in a capacity factor of the power block of 38.6 %.

The second-law analysis of the system in the optimized configuration is conducted to identify the most critical components. A summary is presented in Table 5 while a representation of the exergy streams in the CSP plant is given in Figure 10. The exergy efficiency for each component is calculated as following [44]:

$$\eta = \frac{E_p}{E_f} = 1 - \frac{E_d + E_l}{E_f} \quad (33)$$

where E_p is the exergetic product of the component, E_f are the exergetic resources used to drive it, E_d and E_l represent the exergy destruction and the exergy losses of the component.

Most of the solar exergy hitting the reflectors, i.e. 51.4 %, is lost before reaching the receiver tube due to imperfect concentration. Another big portion is lost or destroyed in the receiver tube such that only 23.3 % of the solar exergy reaches the storage unit. Hence, it is clear that the most critical components are the solar-to-thermal converters. An effective strategy to increase the second-law efficiency of the system is to adopt reflectors with higher optical efficiency and/or multiple axis tracking. This would certainly modify the optimal design of the plant: the increased system products yield per surface ratio would make a larger solar field convenient. On the other hand, most of the exergy optimization studies consider the unit exergetic cost [45] of the functional products as the performance measure of the plant. To this aim, the storage unit, which presents a higher exergetic efficiency, can be improved by reducing the exergy destruction in the thermocline, as shown in [28]. Little room for improvement is left in a mature component like the power block.

Anyhow, the exergetic performance of the system is not considered in the optimization problem formulation and further investigations on this matter are left to future extensions of this work.

The stratified storage has an acceptable exergetic efficiency, i.e. roughly 83 %. This figure of merit allows for a performance comparison between single tank and double tank storage systems. The exergy product of a storage unit can be written in the following form:

$$E_p = \rho_E V \eta \quad (34)$$

where ρ_E is the exergy density of the unit (MWh/m³) and V is the total volume. If the double-tank installation (denoted by the subscript DT) is designed to deliver the same exergy of the single-tank installation (denoted by the subscript ST) we can estimate the required volume ratio as:

$$\frac{V_{DT}}{V_{ST}} = \frac{\rho_{ST} \eta_{ST}}{\rho_{DT} \eta_{DT}} \quad (35)$$

where $\rho_{ST}/\rho_{DT} = 2$. If we consider an ideal (i.e. with 2nd law efficiency equal to unity) double-tank storage system we obtain $V_{DT}/V_{ST} = 1.67$. The additional investment cost of the double-tank alternative results in a LEC of 272.59 \$/MWh, which is 18 % higher than the one obtained with a single-tank system.

Moving to the analysis of economic performances, the system requires a total capital investment of 14.56 million of US\$ and can generate electrical power at the levelized cost of 230.25 \$/MWh. From a comparison with studies on Parabolic Through solar plants ([46-48]), where the estimated LEC ranges from a minimum of 200 \$/MWh to a maximum of 360 \$/MWh for plants sizes in the range of 50 MW_e to 100 MW_e, it is clear that the solution proposed has competitive economic performances.

The CAPEX and LEC breakdown are represented in the pie charts of Figure 11. The cost of the solar field is still the major contributor to the total power plant investment cost accounting for 54% of the total. The second largest item in the plant's owner expenditures list is the power block, which accounts for 15% of the total cost. Finally, the storage tank represents only 10% of the total cost in the optimized configuration. The other pie chart represents the Levelized Electricity Cost breakdown where also the revenues generated from the heat sold on the market are included. In this way, it is possible to notice that cogeneration has the potential to decrease the specific cost of electricity of 28% and this option is thus crucial for the economic viability of small CSP systems.

6.2 Case2

Figure 12 presents the Pareto front obtained from the multi-objective optimization of Case 2. It can be noticed that the minimum possible payback-time found is slightly higher than 6 years and the maximum fraction of thermal load covered by the solar resource that can be reached is very close to 87%. A complete thermal load coverage is extremely non-economical. In order to satisfy completely the winter request, where the thermal load is maximum and the solar yield minimum,

the system would be oversized for most of the year and a large fraction of the thermal energy would not be utilized nor remunerated. The hybridization of the heating and cooling system looks from the curve the most interesting option.

Two extreme points are selected from the Pareto front and their annual performance is analyzed. Point 1 is the most economically viable solution, while the second design, i.e. Point 2, is the one that guarantees the highest solar coverage of the heating and cooling load.

The design specifications and the techno-economic performance of the system in the two selected points are summarized in Table 6. The first issue to notice is that in both points the tracking axis is selected to be East-West oriented. It is well known that this orientation choice guarantees a steadier output throughout the year compared to the N-S counterpart at the price of a lower yearly energy yield. However, we found that the N-S orientation results in a high amount of thermal energy wasted during summer months due to a solar generation that largely exceeds the demand.

The optimal combination of solar multiple, molten salts storage tank size and nominal power of the steam turbine is very interesting. It is found, in fact, that it is more convenient to buy a large steam turbine coupled with a small tank at the cost of a low capacity factor rather than investing in a big storage tank. On the other hand, there are no appreciable differences in the steam generator design between the two Pareto points which confirms the observations of the previous optimization run. The design of point 2 gives a total efficiency decrease of 2%. The electrical capacity factor of the power block is very similar in the two points and differences in the total electricity generation are mainly due to a slight difference in the nominal steam turbine power selected for the optimal design.

The total investment cost of the design in Point 2 is roughly 3.5 M\$ higher than the one in point 1. The difference comes mainly from the solar field cost, from the molten salts storage tank cost and from the water tank cost. The total cost breakdown in the two points is depicted in Figure 13. The relative investment in storage technologies, i.e. water tank and Molten Salts storage tank is nearly 10% higher for Point 2 than for point 1. A larger portion than expected is attributed to the purchase of the hot water storage.

In order to investigate more in details the trends behind the solution found, the system is simulated with different combinations of steam turbine and storage tank sizes. The turbine size is allowed to vary between 1000 kW and 3000 kW with steps of 400 kW, while the tank storage size is allowed to vary between 2 and 18 hours with steps of 4 hours for a total of 20 design points analyzed. The size of the solar field, in terms of mirror area is fixed to 28000 m^2 , as obtained for the design of Point 1. The water tank size is set to a very small value, i.e. 2 hours, in order to exclude the

influence of this parameter on the system performance. All the other parameters are set equal to the design specifications of Point 1.

In all the possible combinations obtained through this procedure, we analyze the normalized breakdown of the power plant revenues, i.e. we consider:

- The incentive-related revenues per unit of investment, in the form of Feed-In-Tariff (FIT) due to the amount of electricity generated
- The heat-related revenues per unit of investment, due to the heat sold to the user.
- The power market-related revenues per unit of investment, due to the selling of power to the electrical grid.

The trend of the FIT-related specific annual revenues per unit of investment $\left[\frac{\$}{\text{year } \$_{inv}}\right]$ for different combinations of the two decision variables selected is depicted in Figure 14.(a). If this was the only earning source of the plant, most convenient designs would be obtained for small steam turbine sizes with big storage tanks. However, by looking at Figure 14.(b), it is clear that specific revenues connected to real market trends are greater for big turbines and for small storage tank size. The reason for such a behavior is that those plants deliver a higher amount of energy right in the middle of the day and thus the average price at which the power is sold is higher. Increasing the operating hours of the steam turbine only adds cost to the system and lower the average price of electricity. As far as the heat-related revenues are concerned (Figure 14(c)), turbine sizes in the range between 1600 kW and 2300 kW are recommended for the hospital considered because higher Thermal Load Capacity Factors can be achieved.

This last analysis shows that the optimal system configuration may vary considerably depending on the incentive policy framework in which the plant is operated.

7 Conclusions

In this paper, we firstly presented an efficient and flexible modeling framework that can accurately predict the performance of the single storage tank with integrated steam generator. In particular, the 1D finite volume model of the steam generator predicts the molten salts temperature with a mean absolute error of 3.16 °C, while the analytic approach used to reduce the CFD model of the tank can reproduce the vertical temperature profile with a mean absolute error of 1.18 °C.

We used this validated model to optimize the system designs in two different cases. In the first case, we optimized the design of a 1MW_e plant located in Rome with an ideal thermal load in order to assess the potential of the technology for mid-size users. We revealed that this type of system could generate power at a price of 230.25\$/MWh, if it is operated for 38% of the year. In particular,

the possibility of utilizing locally the waste-heat, being responsible of a 28 % reduction of the Levelized Cost of Electricity, is crucial for the economic viability of this kind of plants. Furthermore, we found that the single tank configuration with integrated steam generator allows to decrease the specific electricity of another 42 \$/MWh compared to double tank option.

In the second case, we conducted a case-study with a 500 beds Italian hospital with the aim of investigating the performances of the system with a real user in a real market framework. We found that, if the system is properly designed, the investment costs can be recouped in a period between 6 and 7 years and a range between 80% and 87% of the heating and cooling demand can be satisfied with the solar system.

Acknowledgements

The research leading the results reported in this paper has received funding from the European Union's Seventh Framework Program (FP7/2007-2013) under grant agreement n. 268219 for MATS project (Multipurpose Applications by Thermodynamic Solar).

References

- [1] Lilliestam, J., Bielicki, J. M., & Patt, A. G. (2012). Comparing carbon capture and storage (CCS) with concentrating solar power (CSP): Potentials, costs, risks, and barriers. *Energy policy*, 47, 447-455.
- [2] W. Gaggioli and L. Rinaldi, "An Innovative Concept of a Thermal Energy Storage (TES) System Based on the Single Tank Configuration Using Stratifying Molten Salts (MS) as both HSM and HTF, and with an Integrated Steam," in *SolarPACES international Conference 2013*, 2014, pp. 780-789.
- [3] C. Rubbia, "Solar Thermal Energy production: guidelines and future programmes of ENEA" 2001.
- [4] Li, H., Huang, X., & Zhang, L. (2008). A lumped parameter dynamic model of the helical coiled once-through steam generator with movable boundaries. *Nuclear Engineering and Design*, 238(7), 1657-1663.
- [5] Colorado, D., Papini, D., Hernández, J. A., Santini, L., & Ricotti, M. E. (2011). Development and experimental validation of a computational model for a helically coiled steam generator. *International Journal of Thermal Sciences*, 50(4), 569-580.
- [6] Dong, Z., Huang, X., Feng, J., & Zhang, L. (2009). Dynamic model for control system design and simulation of a low temperature nuclear reactor. *Nuclear Engineering and Design*, 239(10), 2141-2151.

- [7] Flueckiger, S. M., Iverson, B. D., Garimella, S. V., & Pacheco, J. E. (2014). System-level simulation of a solar power tower plant with thermocline thermal energy storage. *Applied Energy*, 113, 86-96.
- [8] Yang, Z., & Garimella, S. V. (2010). Thermal analysis of solar thermal energy storage in a molten-salt thermocline. *Solar energy*, 84(6), 974-985.
- [9] Strasser, M. N., & Selvam, R. P. (2014). A cost and performance comparison of packed bed and structured thermocline thermal energy storage systems. *Solar Energy*, 108, 390-402.
- [10] Nithyanandam, K., Pitchumani, R., & Mathur, A. (2014). Analysis of a latent thermocline storage system with encapsulated phase change materials for concentrating solar power. *Applied Energy*, 113, 1446-1460.
- [11] Fornarelli, F., Camporeale, S. M., Fortunato, B., Torresi, M., Oresta, P., Magliocchetti, L., ... & Santo, G. (2016). CFD analysis of melting process in a shell-and-tube latent heat storage for concentrated solar power plants. *Applied Energy*, 164, 711-722.
- [12] Rivas, E., Rojas, E., Bayón, R., Gaggioli, W., Rinaldi, L., & Fabrizi, F. (2014). CFD model of a molten salt tank with integrated steam generator. *Energy Procedia*, 49, 956-964.
- [13] Palenzuela, P., Zaragoza, G., Alarcón, D., & Blanco, J. (2011). Simulation and evaluation of the coupling of desalination units to parabolic-trough solar power plants in the Mediterranean region. *Desalination*, 281, 379-387.
- [14] Darwish, M. A., Abdul-Rahim, H., & Mohtar, R. (2012, October). Doha solar cogeneration power desalting pilot plant: Preliminary design. In *Qatar Foundation Annual Research Forum* (No. 2012).
- [15] Ravaghi-Ardebili, Z., Manenti, F., Corbetta, M., Pirola, C., & Ranzi, E. (2015). Biomass gasification using low-temperature solar-driven steam supply. *Renewable Energy*, 74, 671-680.
- [16] Al-Sulaiman, F. A., Hamdullahpur, F., & Dincer, I. (2012). Performance assessment of a novel system using parabolic trough solar collectors for combined cooling, heating, and power production. *Renewable Energy*, 48, 161-172.
- [17] Buck, R., & Friedmann, S. (2007). Solar-assisted small solar tower trigeneration systems. *Journal of Solar Energy Engineering*, 129(4), 349-354.
- [18] Chacartegui, R., de Escalona, J. M., Sánchez, D., Monje, B., & Sánchez, T. (2011). Alternative cycles based on carbon dioxide for central receiver solar power plants. *Applied Thermal Engineering*, 31(5), 872-879.
- [19] Spelling, J., Favrat, D., Martin, A., & Augsburg, G. (2012). Thermoeconomic optimization of a combined-cycle solar tower power plant. *Energy*, 41(1), 113-120.

- [20] Silva, R., Berenguel, M., Pérez, M., & Fernández-García, A. (2014). Thermo-economic design optimization of parabolic trough solar plants for industrial process heat applications with memetic algorithms. *Applied Energy*, 113, 603-614.
- [21] Fiorenza, G., Sharma, V. K., & Braccio, G. (2003). Techno-economic evaluation of a solar powered water desalination plant. *Energy Conversion and Management*, 44(14), 2217-2240.
- [22] Falchetta, M., Gambarotta, A., Vaja, I., Cucumo, M., & Manfredi, C. (2006). Modelling and simulation of the thermo and fluid dynamics of the “Archimede Project” solar power station. In *Proceedings of ECOS 2006*.
- [23] Srihirin, P., Aphornratana, S., & Chungpaibulpatana, S. (2001). A review of absorption refrigeration technologies. *Renewable and sustainable energy reviews*, 5(4), 343-372.
- [24] F. Zaversky, R. Medina, J. García-Barberena, M. Sánchez, and D. Astrain, “Object-oriented modeling for the transient performance simulation of parabolic trough collectors using molten salt as heat transfer fluid,” *Sol. Energy*, vol. 95, pp. 192–215, Sep. 2013.
- [25] R. Forristall, “Heat Transfer Analysis and Modeling of a Parabolic Trough Solar Receiver Implemented in Engineering Equation Solver Heat Transfer Analysis and Modeling of a Parabolic Trough Solar Receiver Implemented in Engineering Equation Solver,” Tech. Report, Golden, Colorado, 2003.
- [26] Retrieved May 23, 2014, from http://www.soda-is.com/eng/helioclim/helioclim3_eng.html
- [27] Retrieved May 23, 2014, from <https://energyplus.net/weather>
- [28] Pizzolato, A., Verda, V., & Sciacovelli, A.. Local entropy generation analysis of transient processes – an innovative approach for the design improvement of a Thermal Energy Storage with Integrated Steam Generator. *Constructal Law & Second Law Conference 2015 CLC 2015*, Parma (Italy), 18-19 May.
- [29] Dittus, F. W., & Boelter, L. M. K. (1985). Heat transfer in automobile radiators of the tubular type. *International Communications in Heat and Mass Transfer*, 12(1), 3-22.
- [30] Kuppan, T. (2000). *Heat exchanger design handbook* (Vol. 126). New York: Marcel Dekker.
- [31] Chen, J. C. (1966). Correlation for boiling heat transfer to saturated fluids in convective flow. *Industrial & Engineering Chemistry Process Design and Development*, 5(3), 322-329. 25
- [32] Pizzolato, A., Donato, F., Verda, V., & Santarelli, M. (2015). CFD-based reduced model for the simulation of thermocline thermal energy storage systems. *Applied Thermal Engineering*, 76, 391-399.
- [33] J. M. Medina-Flores and M. Picón-Núñez, “Modelling the power production of single and multiple extraction steam turbines,” *Chem. Eng. Sci.*, vol. 65, no. 9, pp. 2811–2820, May 2010.

- [34] H. Hajabdollahi, P. Ahmadi, and I. Dincer, “Thermoeconomic optimization of a shell and tube condenser using both genetic algorithm and particle swarm,” *Int. J. Refrig.*, vol. 34, no. 4, pp. 1066–1076, Jun. 2011.
- [35] S. Pelster, D. Favrat, and M. R. von Spakovsky, “The Thermoeconomic and Environomic Modeling and Optimization of the Synthesis, Design, and Operation of Combined Cycles With Advanced Options,” *J. Eng. Gas Turbines Power*, vol. 123, no. 4, p. 717, 2001
- [36] Spelling, J. (2013). Hybrid Solar Gas-Turbine Power Plants: A Thermoeconomic Analysis, PhD. thesis, Royal Institute of Technology (KTH), Stockholm
- [37] Retrieved May 23, 2014, from <http://www.opts.enea.it/>
- [38] M. Darwish (2012), “Modular Hybridization of Solar Thermal Power Plants For Developing Nations,” M.S. thesis, Royal Institute of Technology (KTH), Stockholm, 2012.
- [39] Turchi, C. (2010). Parabolic trough reference plant for cost modeling with the solar advisor model (SAM) (No. NREL/TP-550-47605). National Renewable Energy Laboratory (NREL), Golden, CO.
- [40] Retrieved October 10,2015, from <http://dgsaie.mise.gov.it/dgerm/prezzigas.asp>
- [41] Retrieved October 10, 2015, from <http://www.mercatoelettrico.org/en/>
- [42] Solar thermodynamic. Retrieved October 12, 2015, from <http://www.gse.it/en/feedintariff/>
- [43]Technology data for energy plants Retrieved June 6, 14, from Energynet.dk
- [44] Bejan, A., &Tsatsaronis, G. (1996). Thermal design and optimization. John Wiley & Sons.
- [45] Lozano, M. A., and A. Valero. "Theory of the exergetic cost." *Energy* 18.9 (1993): 939-960.
- [46] Hinkley, J. T., Hayward, J. A., Curtin, B., Wonhas, A., Boyd, R., Grima, C.,&Naicker, K. (2013). An analysis of the costs and opportunities for concentrating solar power in Australia. *Renewableenergy*, 57, 653-661.
- [47] Kutscher, C., Mehos, M., Turchi, C., Glatzmaier, G., & Moss, T. (2010). Line-focus solar power plant cost reduction plan. Contract, 303, 275-3000.
- [48] International Energy Agency, “Technology Roadmap: Concentrating Solar Power,” OECD Publishing, May 2010

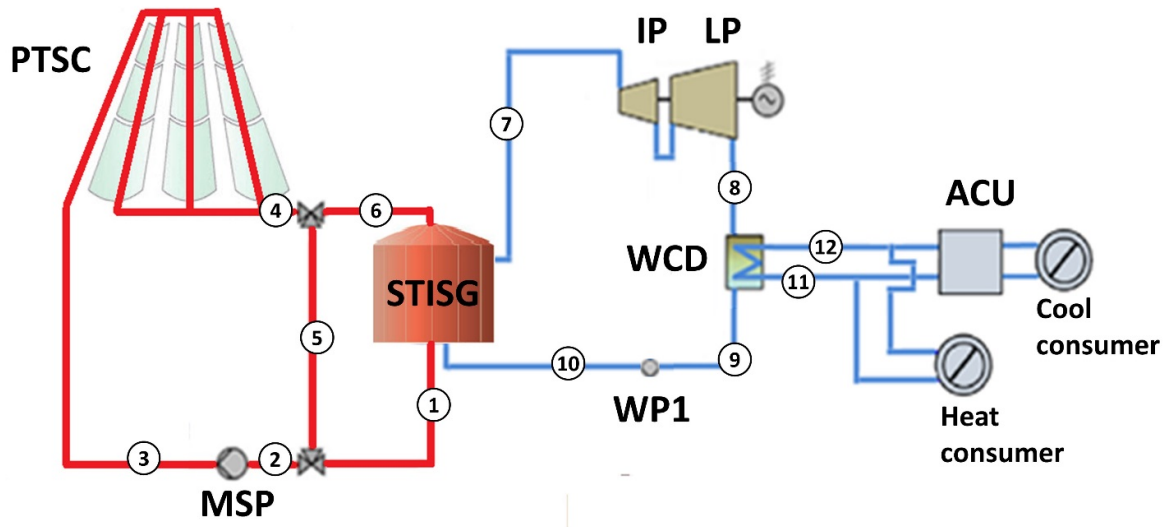


Figure 1. Proposed system layout

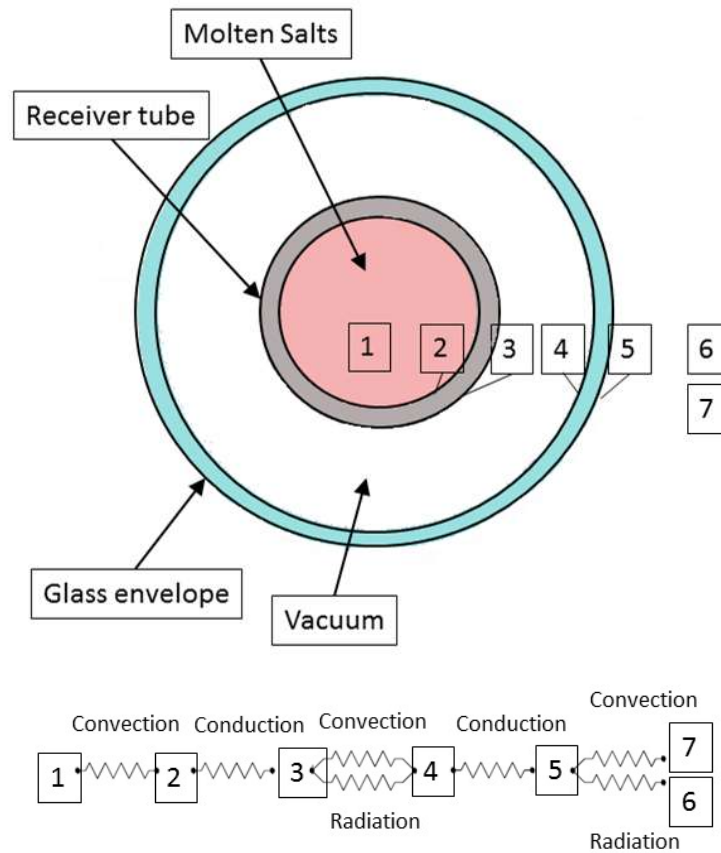


Figure 2. Electrical analogy used to model the heat losses in the receiver tube [22]. (1) Heat Transfer Fluid, (2) absorber inner surface, (3) absorber outer surface, (4) glass envelope inner surface, (5) glass envelope outer surface, (6) air, (7) sky.

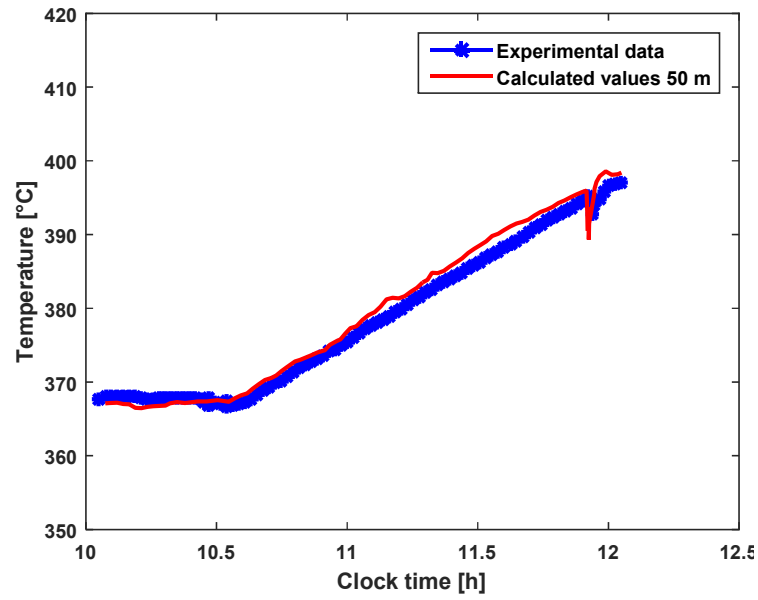


Figure 3. Validation of the solar field model at ENEA Research Center La Casaccia.

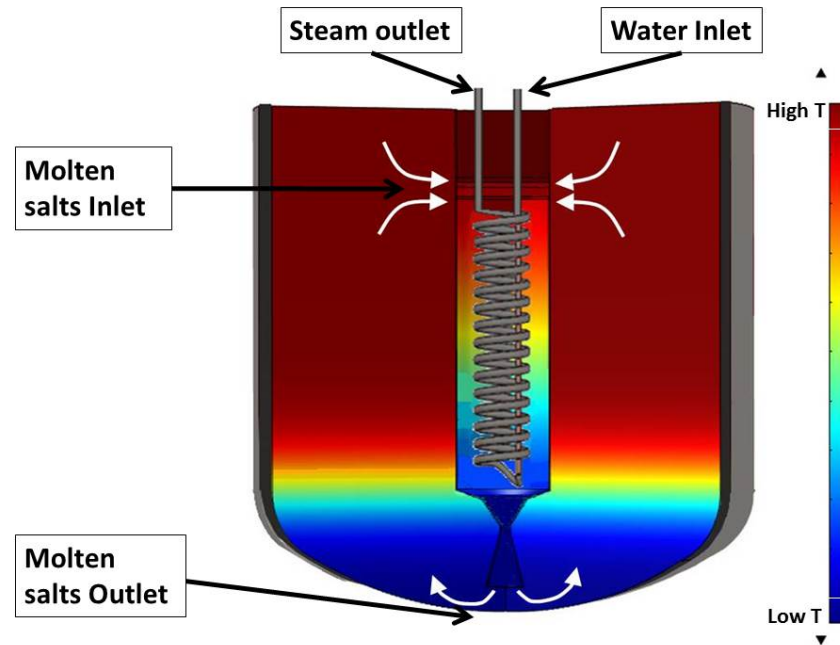


Figure 4. Schematics of the Thermocline TES with integrated Steam Generator

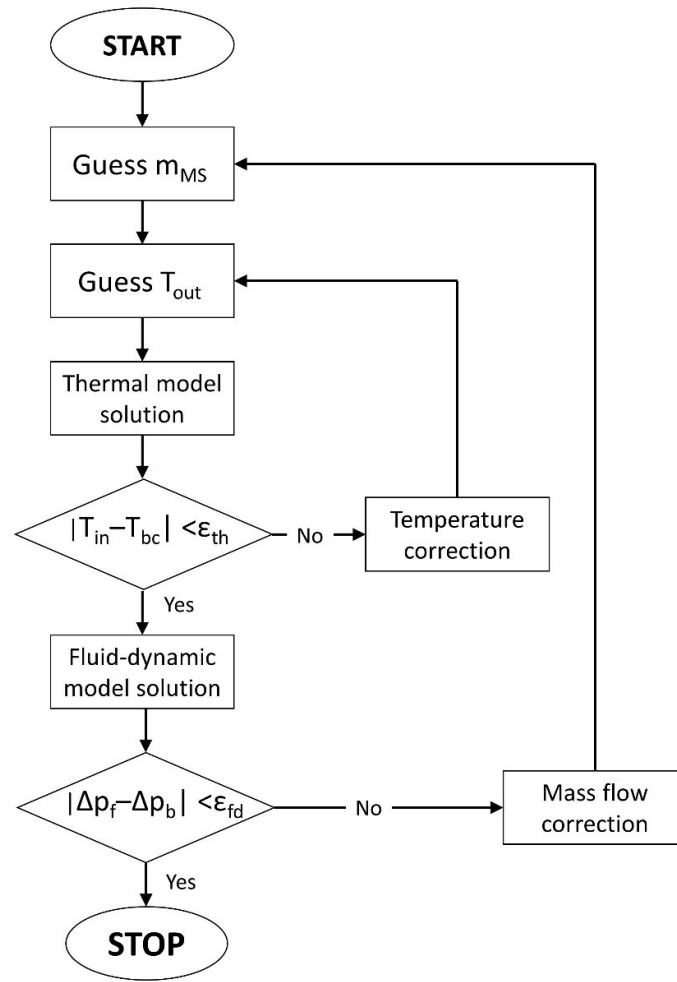


Figure 5. Computational model flow chart of the naturally-circulated steam generator

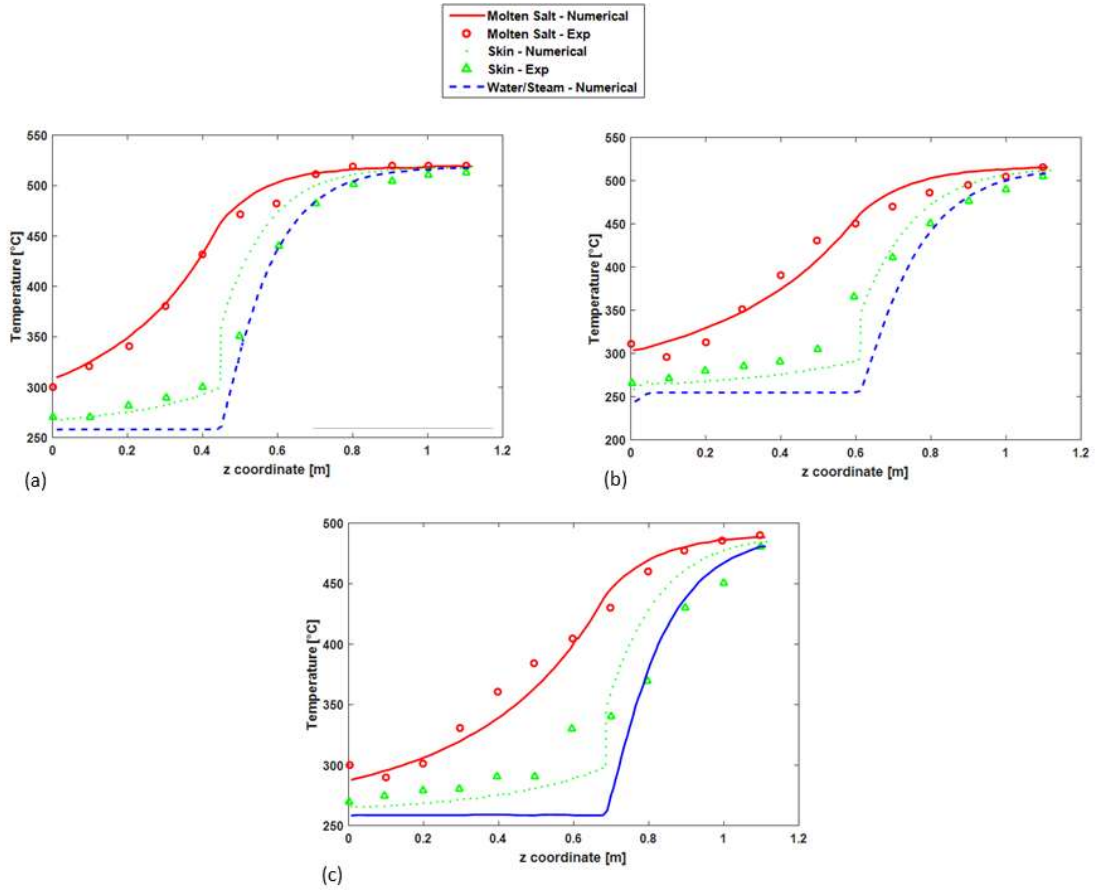


Figure 6. Experimental validation of the steam generator model in three different conditions.(a): 520 °C, 45 bar, mass flow 85% of nominal.(b): 520 °C, 40 bar, mass flow 110% of nominal.(c): 480 °C, 46 bar, mass flow 120 % of nominal

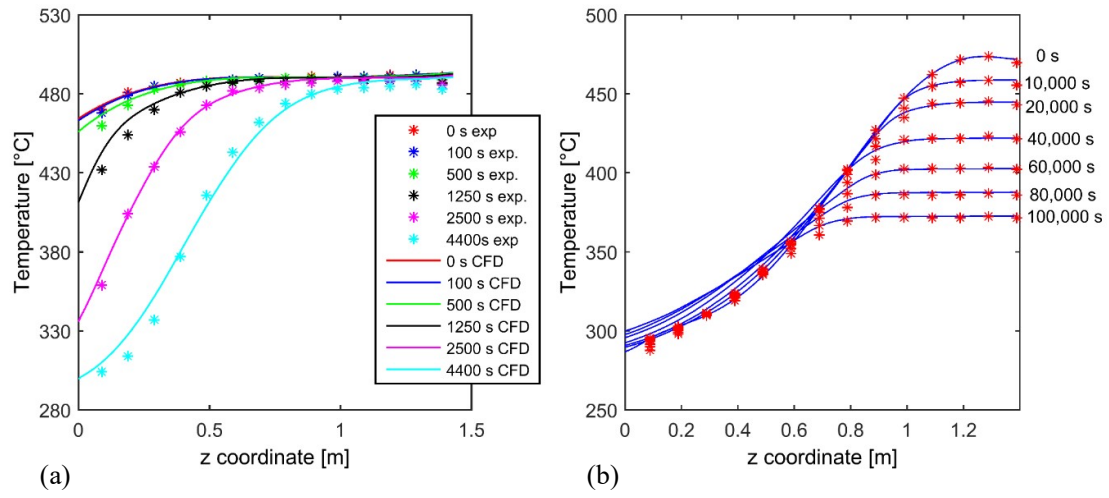


Figure 7. Experimental validation of the CFD model of the storage tank.(a): charging;(b): standby.

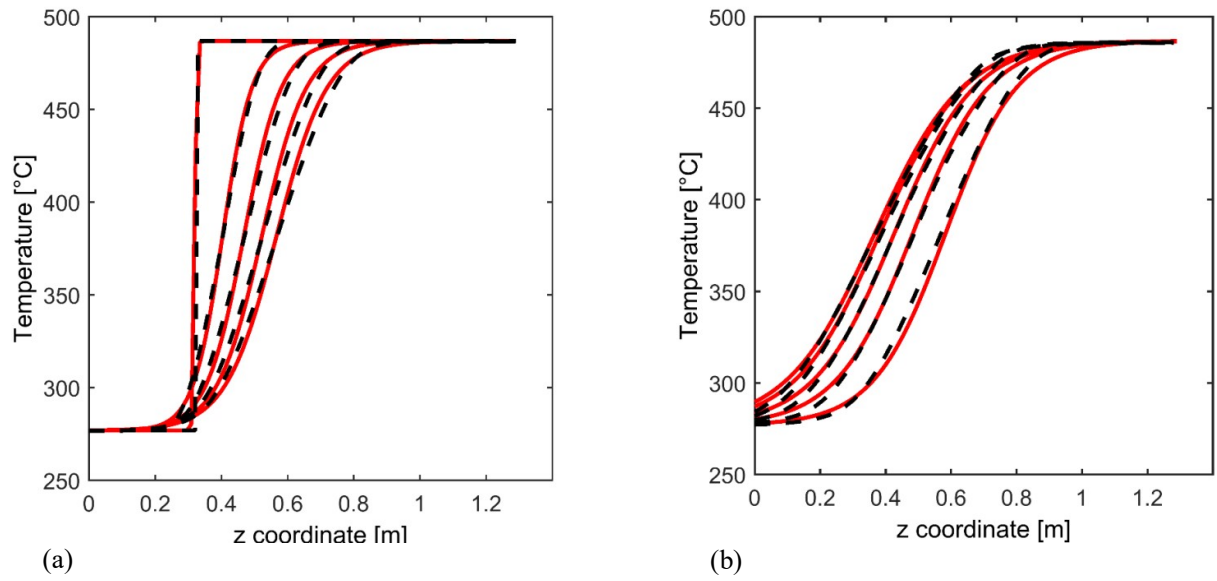


Figure 8. Validation of the reduced model for a continuous process with charging (a) and subsequent discharging (b) Red solid lines are the temperatures profiles obtained through the reduced model while black dotted lines are the ones obtained with the full CFD model[27].

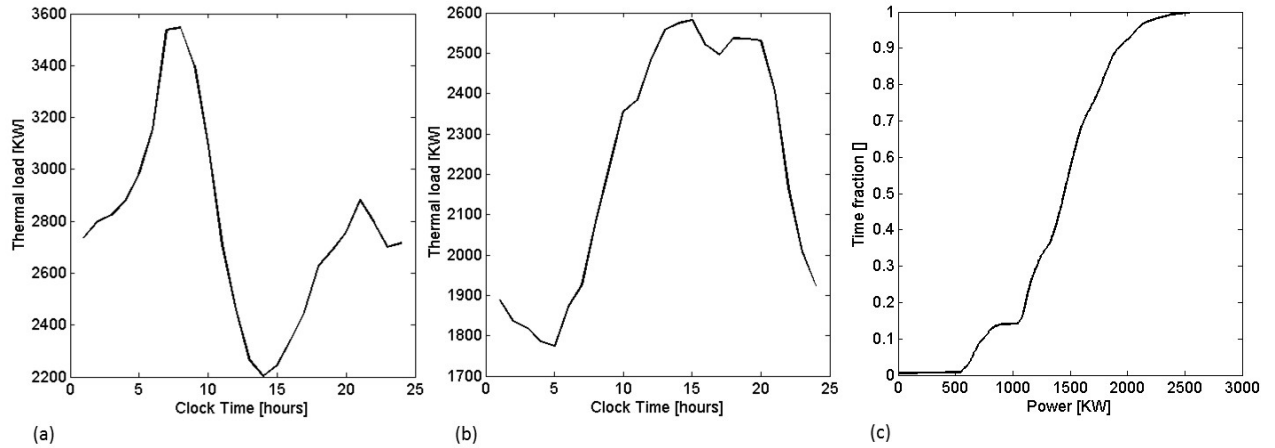


Figure 9. (a): Thermal load on the typical winter day. (b): Thermal load on the typical summer day. (c): Cumulative power distribution in the year considered.

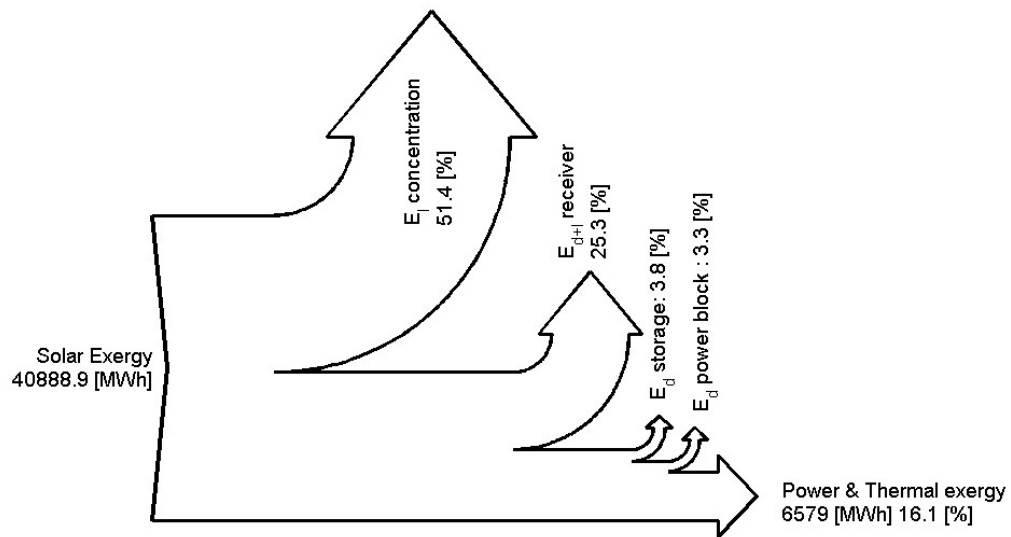


Figure 10. Annual exergy streams of the CSP plant

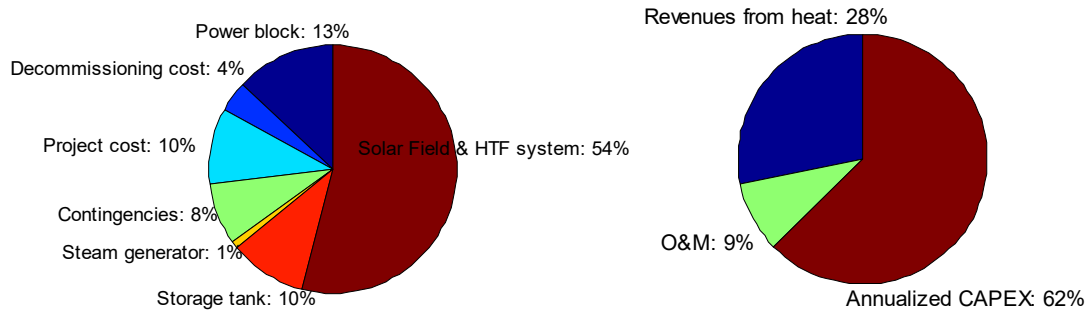


Figure 11. Left: Breakdown of the annualized investment costs, Right: Breakdown of LEC

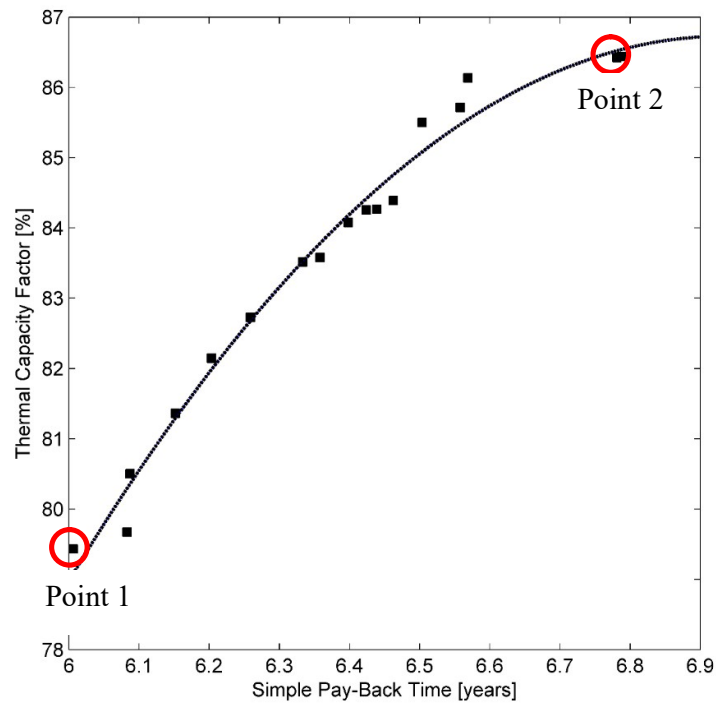


Figure 12. Pareto front: set of solutions of the multi-objective optimizations. Red indicators are obtained by the optimization, the blue solid line is a polynomial regression function used to highlight the trend

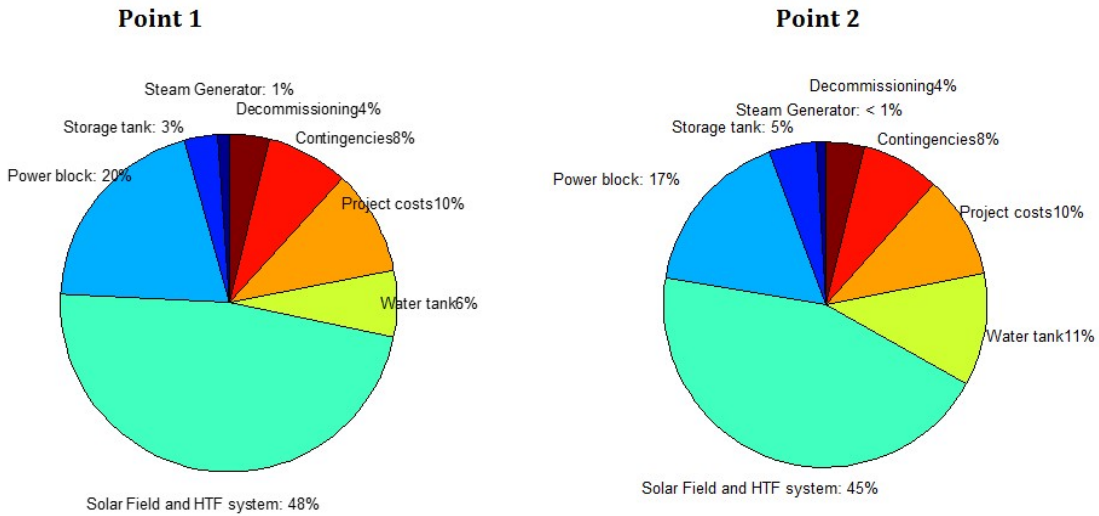


Figure13 Cost breakdown comparison between the two Pareto points selected

Figure

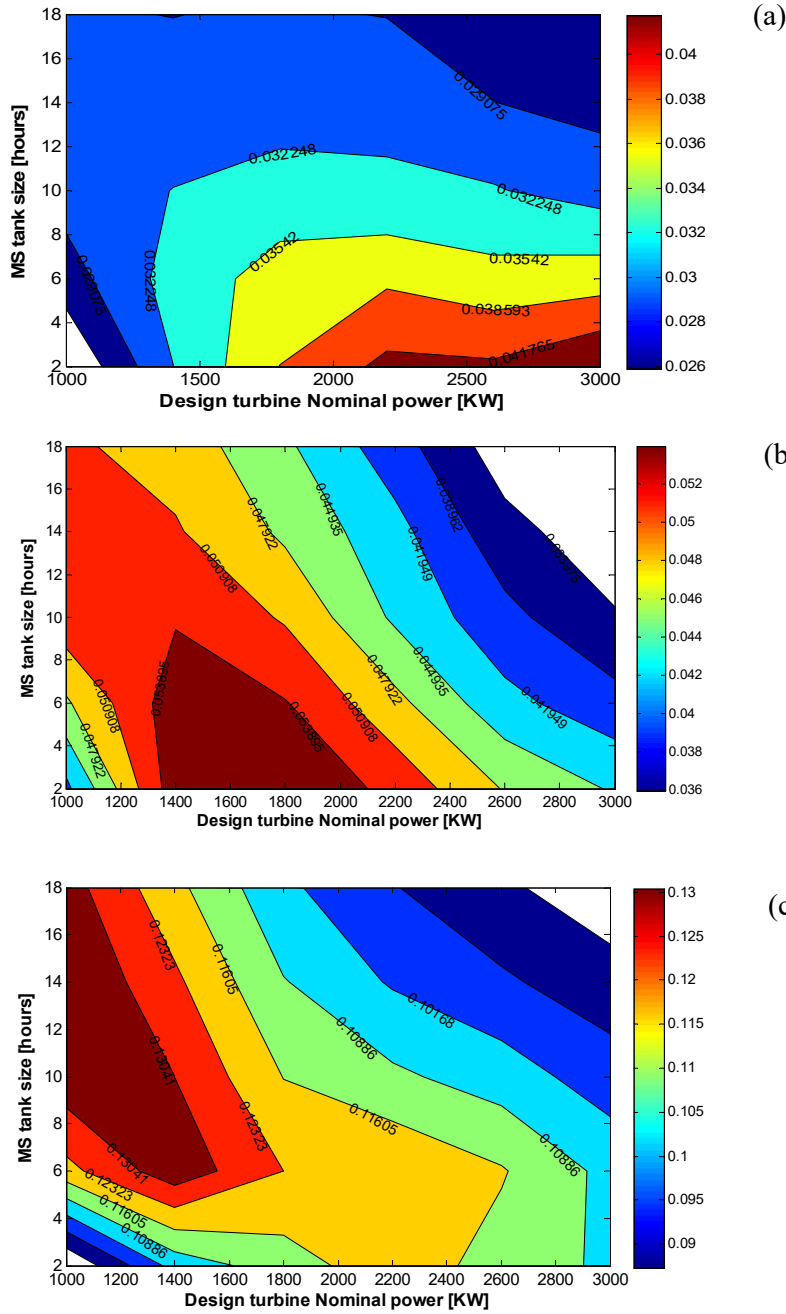


Figure 14. (a):. Revenues from the power market per unit of investment [-]. (b):Revenues from selling heat per unit of investment [-]. (c):Revenues from incentive per unit of investment [-].

Decisionvariable	Lower bound	Upperbound	Type	Utilized in Case 1	Utilized in Case 2
Number of hours of molten storage NH [hours]	1	24	Continuous	Yes	Yes
Tank aspect ratio D/H [-]	0.2	5	Continuous	Yes	Yes
Design Turbine Power P_c [kW]	500	2500	Continuous	No	Yes
Solar Multiple SM [-]	1	8	Continuous	Yes	Yes
Spacing between collectors $d_{spacing}$ [m]	5	25	Continuous	Yes	Yes
Steam generator height H [m]	1	4	Continuous	Yes	Yes
n. of tubes of the steam generator n_{tubes} [-]	3	20	Integers	Yes	Yes
n. of collectors in a string n_{coll} [-]	2	8	Integer	Yes	Yes
Trackingsystemaxis [-]	1 = N-S	2: E-W	Integer	Yes	Yes
Number of hours of water storage NH_{water} [hours]	2	24	Continuous	No	Yes

Table 1. Decision variables overview

DIRECT COSTS	Characteristic dimension	Cost	Unit	n	S_{ref}	Sources
Solar field trough	Mirror surface	357	\$/m ²	1	-	[39] & ENEA
Tank Envelope	External surface	2364	\$/m ²	0.8	1909	[39]
Fluid, Foundations and Handling system (Tank)	Total volume	1131	\$/m ³	0.82	1060	[39] & ENEA
Steam Generator	Number of tubes	11904	\$/ (n _{tubes})	0.78	84	ENEA
Steam turbine	Design electric power	473	\$/MW	0.67	25	[35]
Condenser	Heat transfer surface	585	\$/m ²	1	25	[35]
Pump, BOP, buildings, Safety systems (Power block)	Design electric power	376	\$/MW	0.8	110	[35]
Water tank	Total volume	660	\$/m ³	1		[43] & ENEA
INDIRECT COSTS						
Engineering, Procurement, Construction & Project costs	-	11.8	% of direct capital cost	-	-	[39]
SERVICES and O&M						
Grounds/house keeping	Ground surface	0.04	\$/m ²	-	-	Elaborated from [39]
Mirror washing	Mirror surface	0.41	\$/m ²	-	-	[39]
Water Treatment	Design electric power	1318	\$/MW	-	-	[39]
Materials	-	3.2	% of capital	-	-	[39]

Maintenance			cost			
TES and Power block Labor	Design electric power	5564	\$/ (MW y)	-	-	Elaborated from [39]
Solar field Labor	Mirror surface	2.07	\$/ (m ² y)	-	-	Elaborated from [39]
OTHER COSTS						
Contingencies	-	10	% of total project cost	-	-	[38]
Decommissioning	-	5	% of total project cost	-	-	[38]
Interest rate	-	7	%	-	-	[35]
Insurance rate	-	2	%	-	-	[35]

Table 2. Summary of economic model data

Hours of storage [-]	14.41
Tank Aspect ratio [-]	1.16
Solar multiple [-]	4.12
Mirrorspacing [m]	15.23
Number of collectors per string [-]	8
Height of the steam generator [m]	2.58
Number of tubes of the steam generator [-]	9
Axistracking	N-S

Table 3. Optimal design in the basic configuration

Total power generation [MWh]	3864
Total heatsold [MWh]	10206
Total heatwasted [MWh]	0
Total auxiliaries [MWh]	117
CapacityFactor [%]	38.64
Powerblockefficiency [%]	25.41
Optical efficiency solar field [%]	48.55
Thermal efficiency solar field [%]	80.68
System grosselectricefficiency [%]	9.72
System net electricalefficiency [%]	9.45
System totalefficiency [%]	38.44

Table 4. Energy flows and efficiencies

Exergetic Efficiency of concentrating device[%]	48.56
ExergeticEfficiencyReceiver [%]	47.87
ExergeticEfficiency Storage [%]	83.48
ExergeticEfficiency Turbine [%]	87.50
ExergeticEfficiencyCondenser [%]	84.63
Exergeticefficiency System [%]	16.08

Table 5. Calculated second-law efficiencies of the main components

	Point 1	Point 2
MS storagesize [hours]	1.9	3.2
Design Turbine Power [kW]	2294	2366
Solar multiple [-]	1.87	2.1
HeightSteam Generator [m]	2.69	2.48
Number of tubes steam generator [-]	12	12
Water storagesize [hours]	8.89	18.91
Tracking	E-W	E-W
Direct investment costs [M\$]	16.39	19,95
LEC [\$/MWh]	296	344
Revenues from heat [k\$]	740	794
Revenues from incentive [k\$]	2006	2200
Revenues from market [k\$]	622	738
Simple Pay-Back Time [years]	6.0	6.8
CapacityFactorpowerblock [%]	24.54	24.94
Thermal LoadCapacityFactor [%]	79.22	86.46
Total Power [GWh]	4.71	5.16
Electrical net efficiency [%]	9.32	8.96
Total efficiency [%]	39.62	37.52

Table6. Pareto-pointanalysis